# Temperature-dependent anomalous energy transport in finite-length quasi-one-dimensional $MoS_2$: Crossover from phonons to solitons

Yangjie Wang[1,2,3] and Jige Chen[1,2,*]

[1]*Shanghai Institute of Applied Physics, Chinese Academy of Sciences, Shanghai 201800, China*

[2]*Shanghai Synchrotron Radiation Facility, Zhangjiang Laboratory, Shanghai Advanced Research Institute, Chinese Academy of Sciences, Shanghai 201210, China*

[3]*University of Chinese Academy of Sciences, Beijing 100049, China*

(Received 2 August 2021; revised 16 November 2021; accepted 3 December 2021; published 17 December 2021)

Anomalous energy transport is a widely investigated character in one-dimensional lattice and both phonons and solitons are candidate energy carriers responsible for the thermal conductivity divergence before their mean-free paths. However, it was long believed the contribution of solitons could be neglected even close to the melting point in a real crystalline solid. In this paper, we show that a crossover of wave-packet dynamics, from a phonon- to a soliton-dominated state, occurs in a quasi-one-dimensional molybdenum disulfide ($MoS_2$) sheet at high temperatures far below its melting point by nonequilibrium and equilibrium molecular dynamics simulations. Divergent sound speed variation and the corresponding heat capacity peaks are observed in the transition-temperature region that is related to a second-order phase transition. We also find that its anomalous energy transport falls into a universality class with thermal conductivity divergence exponent $\alpha = 2/5$ at a finite length scale within 2000 nm when solitons are excited above 600 K, and the scaling relations derived from the Lévy walk of energy carriers is fulfilled as $\alpha = 2 - 1/\gamma = \beta - 1$ in the soliton-dominated state above 1800 K. Our results reveal the peculiar solitonlike contribution to thermal conduction at high temperatures in the low-dimensional crystalline solids.

DOI: 10.1103/PhysRevB.104.224306

## I. INTRODUCTION

Anomalous energy transport is a widely investigated and heavily debated signature in theoretical lattice models and real crystalline solids [1–5]. It refers to a breakdown of Fourier' s law in a one-dimensional system, where thermal conductivity $\kappa$ is divergent with system size $L$ as $\sim L^{\alpha}$. Arguments from mode-coupling and renormalization group theories predict three universality classes with $\alpha = 2/5$ [6–14], or $\alpha = 1/3$ (Kardar-Parisi-Zhang, namely, the KPZ universality class) [15–22], or $\alpha = 1/2$ [23–25] in the one-dimensional systems. Thermal conductivity divergence in real finite-length quasi-one-dimensional crystalline solids, such as nanotubes and nanowires, could originate from the finite length before their ultralong mean-free path of energy carriers and their reduced dimensionality. A recent work suggests thermal conductivity of carbon nanotubes converge at an ultrahigh value in millimeter scale (the length scale of its phonon mean-free path) and remains divergent with $\alpha \approx 0.4$ by restraining the flexural motion of carbon atoms as a one-dimensional lattice model [5]. In the microscopic view of thermal conduction, both phonons and solitons could serve as energy carriers in the nonlinear lattice models and crystalline solids. In the low-temperature region, the linear phonon wave packets are dominant energy carriers and the wave-packet dynamics follow the superposition principle. When temperature increases above a critical value, solitons are excited as energy carriers. The superposition principle of wave packets thus fails due to strengthened nonlinearity from solitons. The collision of two solitary wave packets induces a deviation in their respective spatiotemporal trajectories where solitons appear to be instantly translated. The deviation is called a phase shift and it describes the intrinsic nonlinear nature of solitons [14,26–32]. It is thus essential to identify the specific energy carriers and the solitonlike contributions in nonlinear lattices models and crystalline solids beyond the low-temperature region.

However, it was long believed that, as pointed out by Peierls, even close to the melting point the excitations in ordinary three-dimensional crystalline solids are so small that the solitonlike contribution can be neglected [33,34]. Debate about solitonlike contribution also persists in theoretical lattice models. Over a half century ago, to explain the Fermi-Pasta-Ulam (FPU) recurrence, Kruskal and Zabusky derived a Korteweg–de Vries (KdV) equation with supersonic soliton solutions [35]. It is still heavily debated regarding the dominant energy carriers in the FPU lattice to be solitons or phonons (effective phonons with mean-field treatment of nonlinearity) [13,14,29–31,36–39]. The limitation is, even in the integrable Toda lattice, a clear distinction between a phonon and a solitary wave packet is difficult at a low temperature unless the phase shift could be identified [40,41]. Preliminary research suggests strong nonlinearity in some low-dimensional materials like carbon nanotube, graphene, and black phosphorene [42–46], etc. It inspires us to find solitons in a low-dimensional material with a high melting

*chenjige@zjlab.org.cn

 

point, such as molybdenum disulfide ($MoS_2$) that is up to 2648 K [47,48].

Meanwhile, anomalous energy transport could be represented by the Lévy walk of energy carriers, which perform ballistic steps with finite velocity for power-law distributed times [19–21,49–52]. There are thus two scaling relations as

$$\alpha = 2 - \frac{1}{\gamma}, \quad \alpha = \beta - 1. \tag{1}$$

Correlation function of energy $C_E(\delta x, \delta t)$ describes the anomalous energy transport at a given temperature $T$ and gives the scaling exponents $\beta$ and $\gamma$ as [14,36,49–52]

$$C_E(\delta x, \delta t) = \frac{\langle \Delta E(\delta x, \delta t) \Delta E(0,0) \rangle}{\langle \Delta E(0,0) \Delta E(0,0) \rangle} \tag{2}$$

$$\langle \delta x^2 \rangle_E = \int \delta x^2 C_E(\delta x, \delta t) d(\delta x) \sim \delta t^{\beta}, \; C_E(0, \delta t) \sim \delta t^{-\gamma}, \tag{3}$$

where $\langle\rangle$ denotes the ensemble averages, $\Delta E(\delta x, \delta t) = E(\delta x, \delta t) - \langle E(\delta x, \delta t) \rangle$ and $E(\delta x, \delta t)$ denote energy with spatiotemporal intervals $\delta x$ and $\delta t$. $\beta$ describes the superdiffusive behavior from the mean-square displacement (MSD) of energy, and $\gamma$ indicates the separation time between successive ballistic steps of energy carriers as $t^{-1-1/\gamma}$. The KPZ universality class, with energy localized in the hard-point gas or pure solitons in the Toda lattice, obeys the scaling relations as $\alpha = 1/3$, $\beta = 4/3$, and $\gamma = 3/5$ [49,50,52]. The $\alpha = 2/5$ universality class, observed in the FPU lattice with $\alpha = 2/5$ (0.37-0.43) [7,11–14,50], $\beta = 7/5$ (1.4-1.598) [12,14,53], and $\gamma = 0.642 - 0.688$ [50,53], violates the first one with $2 - 1/\gamma > \alpha$ and obeys the latter one $\alpha = \beta - 1$. Some work suggests carbon and Boron nitride nanotubes fall into the $\alpha = 2/5$ (0.38–0.40) universality class and silicon nanowires fall into the KPZ universality class within a long length scale before the mean-free path of energy carriers or by restraining their flexural degree of freedom. However, it is still unknown whether they fulfill the scaling relations [4,5,54,55]. Therefore, it is reasonable to examine the satisfaction of the scaling relations with different energy carriers in various temperature regions.

In this paper, we show a crossover of the wave-packet dynamics from phonons to solitons, which determines the anomalous energy transport behavior at different temperatures in the quasi-one-dimensional $MoS_2$. Nnonequilibrium wave-packet excitations and equilibrium correlations of energy and momentum are studied. To demonstrate the crossover, we define an order parameter through the wave-packets speed and calibrate its corresponding temperature from the sound speed variations. A second-order phase transition from a phonon- to a soliton-dominated state with divergent order-parameter variation is observed at two critical temperatures. The convergence of the scaling exponents obtained at a finite length scale within 2000 nm ($\alpha = 2/5$, $\beta = 7/5$, $\gamma = 5/8$, and thus $\alpha = 2 - 1/\gamma = \beta - 1$) occurs at a high temperature far below the melting point.

## II. ANALYTIC AND NUMERIC MODELING

Hamiltonian of the Mo-S system, based on the reactive empirical bond-order (REBO) potential [56–58], has the form as

$$H = \sum_i \frac{p_i^2}{2m_i} + \sum_{i \neq j, j>i} f_{ij}^C(r_{ij}) [V^R(r_{ij}) - b_{ij} V^A(r_{ij})], \tag{4}$$

where $p_i$ and $m_i$ denote the momentum and mass of the $i$th atom, and $r_{ij}$ is the interatomic separation between the $i$th and the $j$th atoms; $f_{ij}^C(r_{ij})$ is the cutoff function, $V^R(r_{ij})$ and $V^A(r_{ij})$ are the pairwise repulsion and attraction, and $b_{ij}$ is the bond-order term. By simplifying the quasi-one-dimensional $MoS_2$ as a one-dimensional lattice along the $x$ axis, we derive a KdV equation and a supersonic soliton solution as

$$\dot{r_1} + \frac{2v_0 k_2}{k_1} r_1 r_1' + \frac{v_0}{6} r_1''' = 0,$$
$$r_1 = \frac{3v_s k_1}{4v_0 k_2} \mathrm{sech}^2 \sqrt{\frac{3v_s}{2v_0}} (\varsigma - v_s \tau), \tag{5}$$

where coordinates are transformed by a perturbation coefficient $\varepsilon$ as $\varsigma = \varepsilon^{\frac{1}{2}}(x - v_0 t)$ and $\tau = \varepsilon^{\frac{3}{2}} t$; $r_1$ denotes the zero order of atomic displacement, $\dot{r_1}$ denotes its partial derivative of $\tau$, $r_1'$, and $r_1'''$ denotes its first- and third-order partial derivatives of $\varsigma$; $k_1$, $k_2$, and $v_0$ are constants; and $v_s$ is soliton velocity. Therefore, the analytical feasibility of finding solitons is guaranteed and the complete derivation is given in the Appendix.

For numerical modeling, we have performed both nonequilibrium and equilibrium molecular dynamics simulations. The schematic is illustrated in Fig. 1(a) and the dimension of the quasi-one-dimensional $MoS_2$ sheet is $240 \times 1.5\ \mathrm{nm}^2$, with the armchair direction along the $x$ axis and the zigzag direction along the $y$ axis. Periodic boundary conditions are used in the $x - y$ plane. Liang *et al.* developed a potential in 2009 combining a REBO potential and Lennard-Jones (LJ) potential for Mo-S systems [56,57]. Later, Stewart and Spearot modified this potential and made an open source implementation within LAMMPS [59,60]. This version of REBO potential, which is believed to be reliable in describing thermal and anharmonic properties of $MoS_2$, is used in our simulations [58–60]. Here the LJ potential part is excluded since only the single-layer $MoS_2$ is concerned in our study. Similar to literature, the in-plane pressure of zero and a time step of 0.5 fs are used in our simulations. Wave packets are excited by adding velocity $\chi_L$ or $-\chi_R$ km/s along the $x$ axis on an array of atoms (covered in the red box). Kinetic energy excitation $\delta E_k(x,t)$ characterizes the spatiotemporal trajectories of the wave packets. Correlation functions of momentum [$C_{p_x}(\delta x, \delta t)$ and $C_{p_y}(\delta x, \delta t)$] and energy [$C_{E_k}(\delta x, \delta t)$ and $C_E(\delta x, \delta t)$] are calculated in the same manner in Eq. (1) as [14,36,39,45,61]

$$\delta E_k(x,t) = E_k(x,t) - E_{k0}(x,t),$$
$$C_{p_x}(\delta x, \delta t) = \frac{\langle \Delta p_x(\delta x, \delta t) \Delta p_x(0,0) \rangle}{\langle \Delta p_x(0,0) \Delta p_x(0,0) \rangle},$$
$$C_{p_y}(\delta x, \delta t) = \frac{\langle \Delta p_y(\delta x, \delta t) \Delta p_y(0,0) \rangle}{\langle \Delta p_y(0,0) \Delta p_y(0,0) \rangle},$$
$$C_{E_k}(\delta x, \delta t) = \frac{\langle \Delta E_k(\delta x, \delta t) \Delta E_k(0,0) \rangle}{\langle \Delta E_k(0,0) \Delta E_k(0,0) \rangle}, \tag{6}$$

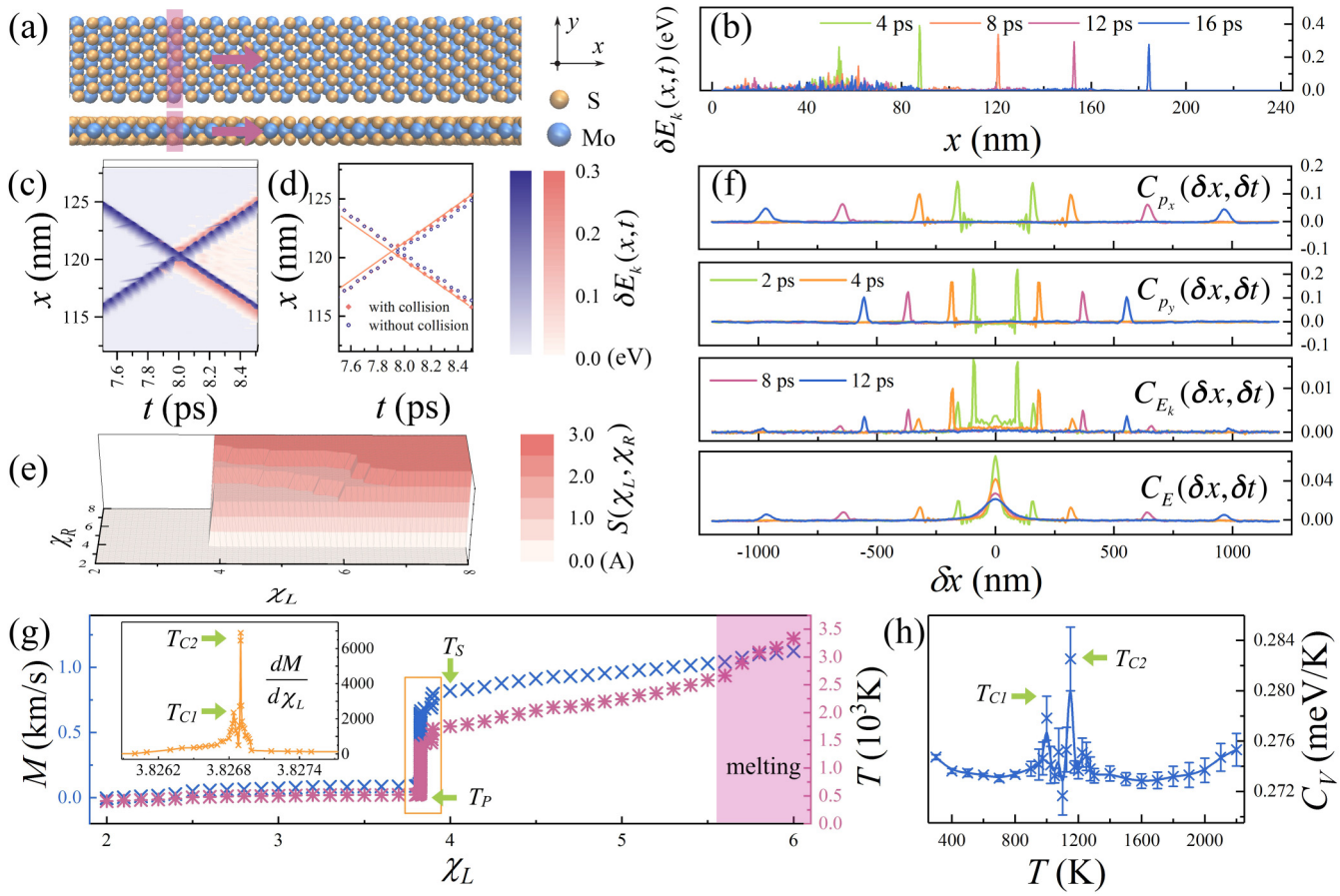


FIG. 1. (a) Schematic of wave-packet excitation in the quasi-one-dimensional $MoS_2$. The sheet is placed with the armchair direction along the $x$ axis and the zigzag direction along the $y$ axis. A heat pulse (red arrow) excites wave packets by adding velocity $\chi_L$ or $-\chi_R$ km/s along the $x$ axis on an array of atoms (covered in the red box). (b) Time variation of an advancing wave packet characterized by the kinetic energy excitation $\delta E_k(x,t)$, excited by $\chi_L$=5 at $x$=50 nm. (c, d) Spatiotemporal trajectories of two solitons with head-on collision, simultaneously excited by $\chi_L$=5 at $x$=50 nm and $-\chi_R$=-5 at $x$=190 nm, are colored in orange. Their separate trajectories without collision are colored in blue. Trajectories of soliton peaks are plotted in (d) and the solid lines represent the extended trajectories of wave packets after collisions. (e) phase-shift strength of two collided wave packets, measured by the spatial translation $S(\chi_L, \chi_R)$ in the unit of periodic cell length A, as a function of $\chi_L$ and $\chi_R$. (f) Time variation of correlation functions, $C_{p_x}(\delta x, \delta t)$ and $C_{p_y}(\delta x, \delta t)$ of longitudinal and transverse momentum, and $C_{E_k}(\delta x, \delta t)$ and $C_E(\delta x, \delta t)$ of kinetic energy and total energy at 2000 K. (g) The order-parameter $M = v_l(\chi_L) - v_l(2)$ and $v_l(\chi_L)$ being the longitudinal wave-packet speed as a function of $\chi_L$. The corresponding temperature $T$ is calibrated from the inverse function of sound speed $u_l(T)$ and using the equality $u_l = v_l$. $T_P < T < T_S$ refers to the transition-temperature region (covered in the empty box);$T_{C1}$ and $T_{C2}$ refer to temperatures with divergent $dM/d\chi_L$. The melting-temperature region is covered in the red box. (h) Specific heat capacity $C_V = \partial E/\partial T$ as a function of $T$.

where $E_k(x,t)$ represents the kinetic energy of atoms with an initial excitation and $E_{k0}(x,t)$ represents the kinetic energy by excluding the initial excitation; $p_x(\delta x, \delta t)$ and $p_y(\delta x, \delta t)$ denote the longitudinal and transvers momentum; and $E_k(\delta x, \delta t)$ denotes the kinetic energy between atoms with spatiotemporal intervals $\delta x$ and $\delta t$. To our best computation capacity, we use 100 K intervals (25 K intervals in the transition-temperature region) from 300 to 2400 K in the equilibrium simulations. To obtain $\kappa$ and $\alpha$, we use the reverse nonequilibrium molecular dynamics [62] and vary the length $L$ from 30 to 240 nm {and a longest length 2000 nm is considered in our thermal conductivity calculations. Thickness of the $MoS_2$ sheet is chosen as the bulk layer separation distance 0.615 nm [58,63]. The calculated value of $\kappa$ is consistent with results in the literature by using a SW (Stillinger-Weber) potential for the Mo-S system [58,64]; please see details in the Supplemental Material [65]}.

## III. RESULTS AND DISCUSSION

As shown in Fig. 1(b) and Fig. 2, a longitudinal soliton wave packet, characterized by the kinetic energy excitation $\delta E_k(x,t)$ or the longitudinal momentum excitation $\delta p_x(x,t)$, could be excited by $\chi_L = 5$ or 8 at $x = 50$ nm and it leaves a phonon tail far behind, which is similar to soliton excitation in the FPU and Toda lattices [30–32]. The contribution from the nonlinear terms is strong enough to excite solitons. Solitons are supersonic (larger than the sound speed in the harmonic limit under a infinite small $\chi_L$) and thus leave the phonon tail far behind. On the other hand, when the excitation strength is

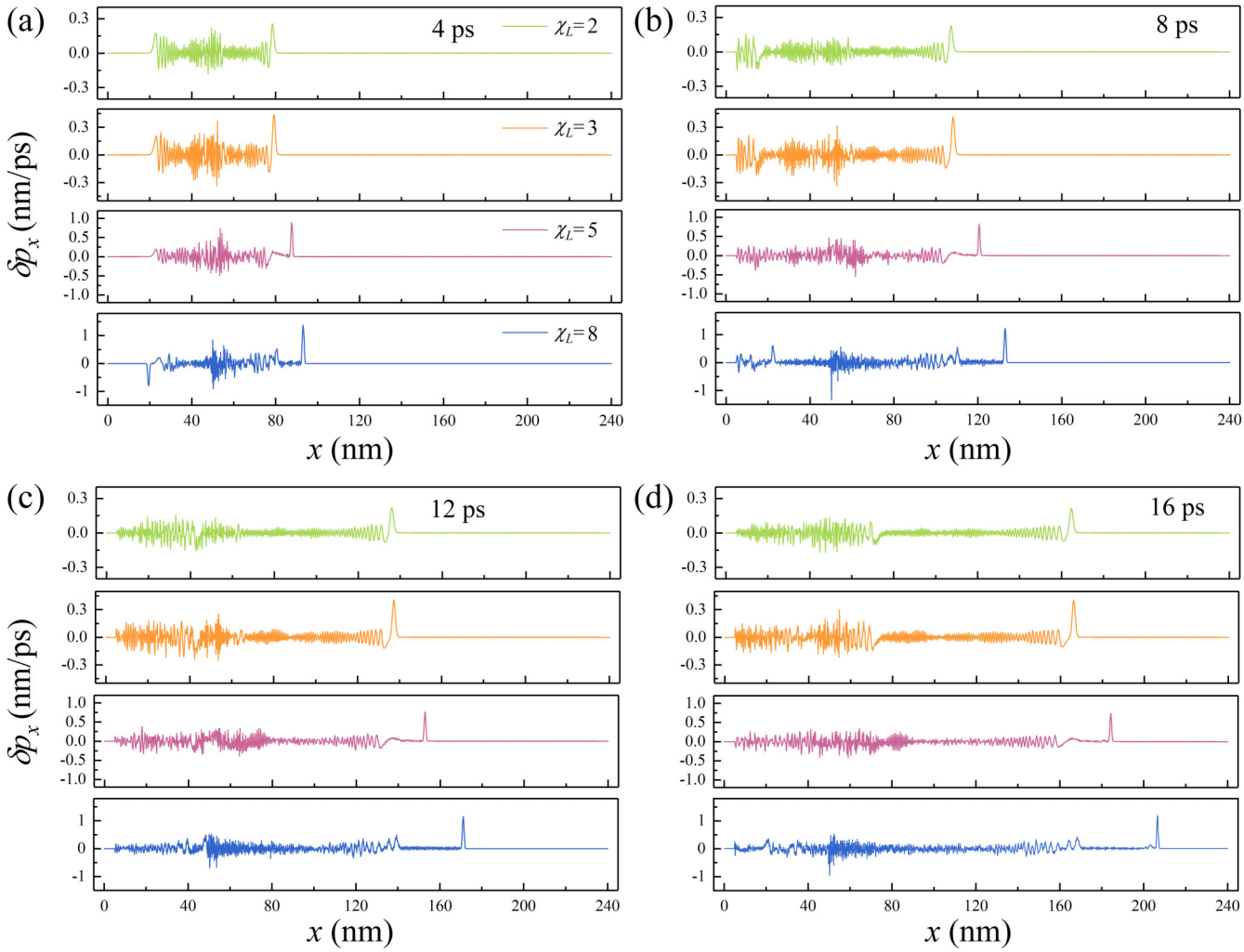


FIG. 2. (a–d) Time variation of the longitudinal wave packets identified by $\delta p_x$ and excited by $\chi_L = 2$ and 3 (phonon wave packets), 5 and 8 (soliton wave packets), at $x = 50$ nm.

comparatively small, the harmonic part of atomic interactions would play the dominant role in determining the excited wave-packet profile. For a weak excitation $\chi_L = 2$ or 3 ($\chi_L < 3.83$), the phonon tail closely follows the advancing wave packet, which is similar to the phonon excitation in the harmonic lattice. Their advancing speeds are small and almost identical to the sound speed in the harmonic limit. We denote the wave-packet speed as $v_l(\chi_L)$ and it represents the upper limit of energy transport speed under different excitation strength. In the equilibrium state, the upper limit refers to the longitudinal sound speed $u_l(T)$ at the given temperature $T$. Later we use the equality $u_l = v_l$ to associate the nonequilibrium and equilibrium wave-packet dynamics together. As shown in Figs. 2(a)–2(d), the advancing speed of the wave-packet $v_l(\chi_L)$ follows the relation that $v_l(8) > v_l(5) > v_l(3) \approx v_l(2)$ since the advancing speeds of soliton wave packets are dependent on its excitation strength while the phonon wave packets are almost identical due to their weak nonlinearity. We have also observed the excitation of transverse wave packets; see PS1 in the Supplemental Material [65]. To identify the soliton nature of a wave packet, it is necessary to perform the collision between two wave packets. Phase shift is the intrinsic property of solitons and it describes the asymptotic interaction between solitons. Consistently, we perform the head-on collision between wave packets excited by $\chi_L$ and $-\chi_R$ from 2 to 8. As shown in Figs. 1(c) and 1(d) and 3(b) and 3(d), the spatiotemporal trajectories of two simultaneously excited wave packets ($\chi_L = 5$ at $x = 50$ nm and $-\chi_R = -5$ at $x = 190$ nm) are colored in orange. To make a comparison, their separate trajectories, independently excited in another two systems, are colored in blue in the same plot. Before collision ($0 < t < 7.95$ ps), the wave-packet trajectories with and without collisions are identical. Phase shift occurs at 7.95 ps. The collided wave-packet peaks appear to be instantly translated 3/2 periodic cells forward and it implies the two wave packets are solitons under this excitation strength. After collision ($t > 7.95$ ps), by extending trajectories of the wave packets after collision [indicated by the solid lines in Fig. 1(d)], a clear spatiotemporal deviation between wave packets with and without collision is observed. On the other hand, as illustrated in Figs. 3(a) and 3(c), no spatiotemporal deviation is observed between wave packets excited by $\chi_L = 2$ and $-\chi_R = -2$. The spatiotemporal trajectories of the collide-wave packets show no deviation from their separate trajectories without

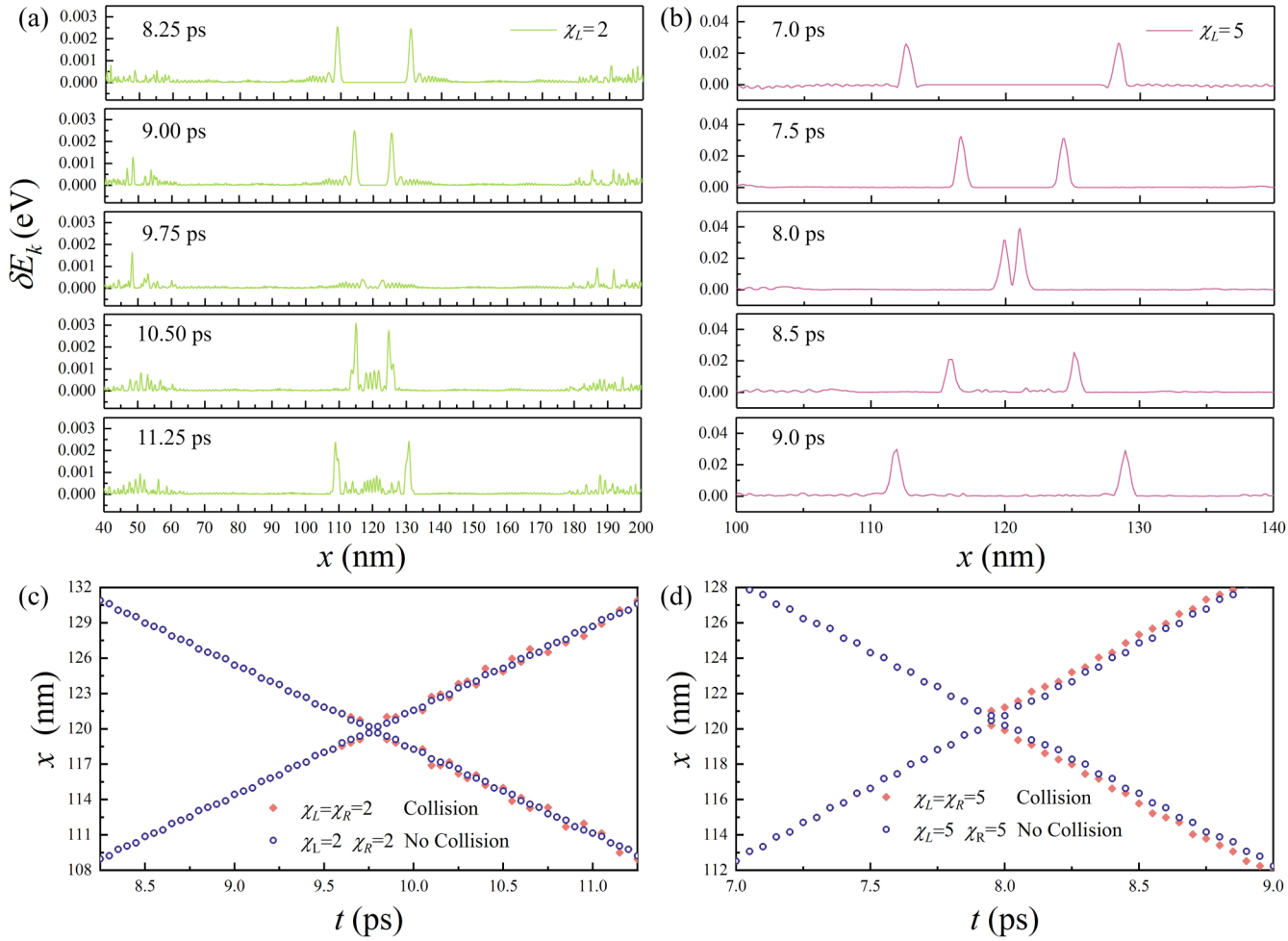


FIG. 3. (a, b) Time variation of two wave- packets with head-on collision, simultaneously excited by $\chi_L = 2$ and $-\chi_R = -2$ (collision of two phonon wave packets), and $\chi_L = 5$ and $-\chi_R = -5$ (collision of two soliton wave packets). (c, d) Trajectories of the wave-packet peaks are colored in orange. As a comparison, the separate trajectories of wave packets without collision independently excited by $\chi_L$ and $-\chi_R$, are colored in blue.

collision. It indicates that the superposition principle is fulfilled at this small excitation strength. Meanwhile, phase-shift strength is usually measured by the spatial translation length $S(\chi_L, \chi_R)$ [26,28,30,32] in the unit of a periodic cell length (A = 0.548 nm). As shown in Fig. 1(e), nonzero $S(\chi_L, \chi_R)$ is observed until $\chi_L \geqslant 3.83$ and $\chi_R \geqslant 3.83$. Threshold of soliton excitation strength is thus 3.83. No phase shift occurs at collision between phonon-phonon ($\chi_L < 3.83$ and $\chi_R < 3.83$) and phonon-soliton ($\chi_L < 3.83$ or $\chi_R < 3.83$) wave packets.

The correlation functions describe the spreading of the initial energy and momentum fluctuations at a given temperature. As illustrated in Fig. 1(f) and Fig. 4(a), the longitudinal and transverse momentum correlations at a high temperature like 2000 K, $C_{p_x}(\delta x, \delta t)$ and $C_{p_y}(\delta x, \delta t)$, exhibit two symmetric advancing fronts induced by the fastest energy carriers. The high-temperature behavior is similar to soliton-involved correlations in the FPU and Toda lattices [31,36–39,51]. On the other hand, as illustrated in Fig. 4(b), the low-temperature behavior, e.g., at 300 K, is similar to correlations in the harmonic lattice with vibrational fronts. Longitudinal and transverse fronts also appear in the kinetic energy and energy correlations $C_{E_k}(\delta x, \delta t)$ and $C_E(\delta x, \delta t)$. Later, the scaling exponents $\beta$ and $\gamma$ are obtained by calculating $C_E(\delta x, \delta t)$ at different temperatures. Longitudinal and transverse sound speeds, $u_l(T)$ and $u_t(T)$, are obtained by measuring the peak position of the advancing fronts [14,36–38]. The temperature-dependent sound speed variation is presented in PS2 in the Supplemental Material [65].

It is known that the increase of sound speed with temperature is entirely caused by the strengthened nonlinearity. Consistently, we define an order-parameter $M = v_l(\chi_L) - v_l(2)$ to measure the nonlinearity strength in the wave-packet excitations. The equilibrium temperature is thus calibrated from the inverse function of longitudinal sound speed $u_l(T)$. By using the equality $u_l = v_l$, we could associate an equilibrium temperature $T$ with an order-parameter $M$. As illustrated in Fig. 1(g), $M$ exhibit a crossover from phonons- to solitons-dominated state as a function of $\chi_L$.

(i) In the low-temperature region ($\chi_L$<3.83, $T < T_P$, $T_P$ = 548.5 K), $M$ is approximately constant to be zero since only phonons are excited. The sound speed is almost invariant due to the weak nonlinearity in this phonon-dominated state.

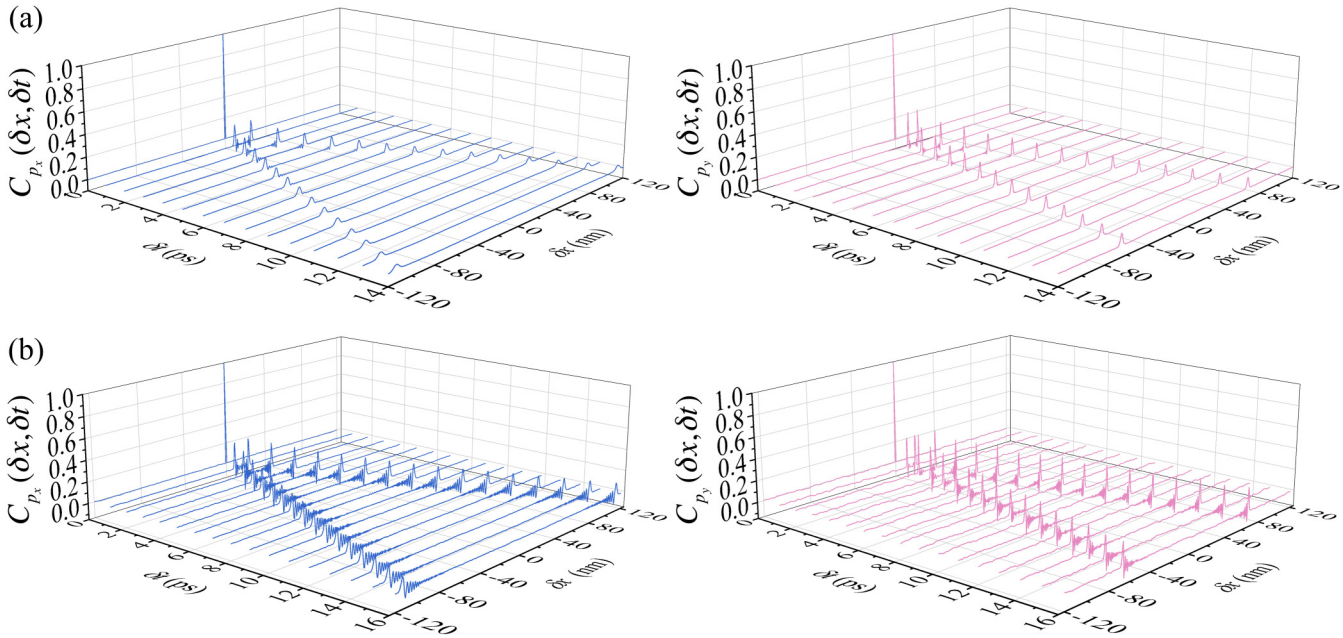


FIG. 4. (a, b) Time variations of the correlation functions of longitudinal and transverse momentum $C_{p_x}(\delta x, \delta t)$ and $C_{p_y}(\delta x, \delta t)$ at (a) a high temperature 2000 K and (b) a low equilibrium temperature 300 K.

(ii) In the transition-temperature region ($3.83 \leqslant \chi_L < 4.00$, $T_P \leqslant T < T_S$, $T_S = 1753$ K), $M$ suddenly jumps to a high value since solitons are excited. Its variation rate $dM/d\chi_L$ becomes divergent near $\chi_L = 3.82684$ ($T_{C1} = 959$ K) and 3.82690 ($T_{C2} = 1149.5$ K). It resembles a second-order phase transition with two critical points. We conjecture two instead of one critical points is due to the quasi-one-dimensional structure where both longitudinal and transverse energy transport are involved.

(iii) In the high-temperature region ($\chi_L \geqslant 4.00$ and $T > T_S$), $M$ increases linearly with $\chi_L$ where solitons become the dominant energy carriers with linear-increased wave-packet speed. $T_S$ (1753 K) is still far below the melting point at 2648 K [48].

Now let us consider how the crossover affects the heat capacity of $MoS_2$. Here the specific heat capacity $C_V = \partial E/\partial T$ is calculated at constant volume since periodic boundary conditions are applied and $C_V = 0.318$ meV/K at 300 K. As illustrated in Fig. 1(h), two peaks are observed in the transition-temperature region near $T_{C1}$ (1000 K) and $T_{C2}$ (1150 K). We thus conjecture that this crossover is related to a second-order phase transition. However, limited by our computation accuracy, we cannot conclude $C_V$ is also divergent at $T_{C1}$ and $T_{C2}$ and more rigid analysis is needed.

Now we turn to the scaling exponents in the anomalous energy transport of the quasi-one-dimensional $MoS_2$ at a finite length scale within 2000 nm. As illustrated in Figs. 5(a)–5(c), similar power-law behaviors, like anomalous energy transport in the one-dimensional nonlinear lattice models, are observed. Here $\kappa$ is divergent as $\sim L^{\alpha}$ (calculation details of $\kappa$ are given in PS3 in the Supplemental Material [65]), $C_E(0, \delta t)$ decays as $\sim \delta t^{-\gamma}$, and $\langle \delta x^2 \rangle_E$ is superdiffusive as $\sim \delta t^{\beta}$ ($\beta$ is fitted before the advancing fronts reaching the boundaries). In particular, the three scaling exponents are found to be temperature dependent rather than invariant constants. As illustrated in Figs. 5(d) and 5(e), variations of three scaling exponents and their scaling relations $\alpha = 2 - 1/\gamma = \beta - 1$ at different temperatures are studied. It is found that (1) $\alpha$ varies from 4/5 to 2/5 from 300 to 600 K. It converges to 2/5 when $T \geqslant 600$ K (above $T_P$); (2) $\gamma$ varies from 1 to 5/8 from 300 to 1800 K. It converges to 5/8 and thus $2 - 1/\gamma = \alpha = 2/5$ is fulfilled when $T \geqslant 1800$ K (above $T_S$). (3) $\beta$ equals 8/5 at 300 K and exhibits two peak values near $T_{C1}$ and $T_{C2}$. It converges to 7/5 and thus $\beta - 1 = \alpha = 2/5$ is fulfilled when $T \geqslant 2000$ K (above $T_{S*}$). Therefore we could see that variation of the scaling exponents is related to the crossover of wave-packet dynamics from phonons to solitons. The quasi-one-dimensional $MoS_2$ falls into the $\alpha = 2/5$ universality class when solitons start becoming energy carriers above 600 K and both phonons and solitons act as energy carriers. The excitation of solitons leads to an invariant $\alpha$ within a microscopic length scale of several hundreds nanometers. The first scaling relation $\alpha = 2 - 1/\gamma$ is fulfilled when solitons become the dominant energy carriers above 1800 K and it resembles the pure-soliton behavior in the Toda lattice [50,52]. The second scaling relation $\alpha = \beta - 1$ is also fulfilled in the soliton-dominated temperature region. But why the convergent temperature 2000 K ($T_{S*}$) is a bit higher than $T_S$ remains to be understood. Furthermore, since $\beta = 2$ means ballistic transport, we use $1/(2 - \beta)$ in Fig. 5(e) to indicate the possible divergence of MSD near $T_{C1}$ and $T_{C2}$ in Fig. 5(e). Again, the two peaks suggest this crossover is related to a second-order phase transition near the critical temperatures. Similar results are observed in the quasi-one-dimensional $MoS_2$ with different chirality (see PS4 in the Supplemental Material [65]).

Here it should be emphasized that the anomalous energy transport and the relative scaling exponents in this work are obtained within a finite-length scale. It is intended to understand the temperature-dependent variation of energy carriers and their relative wave-packet dynamics in $MoS_2$.

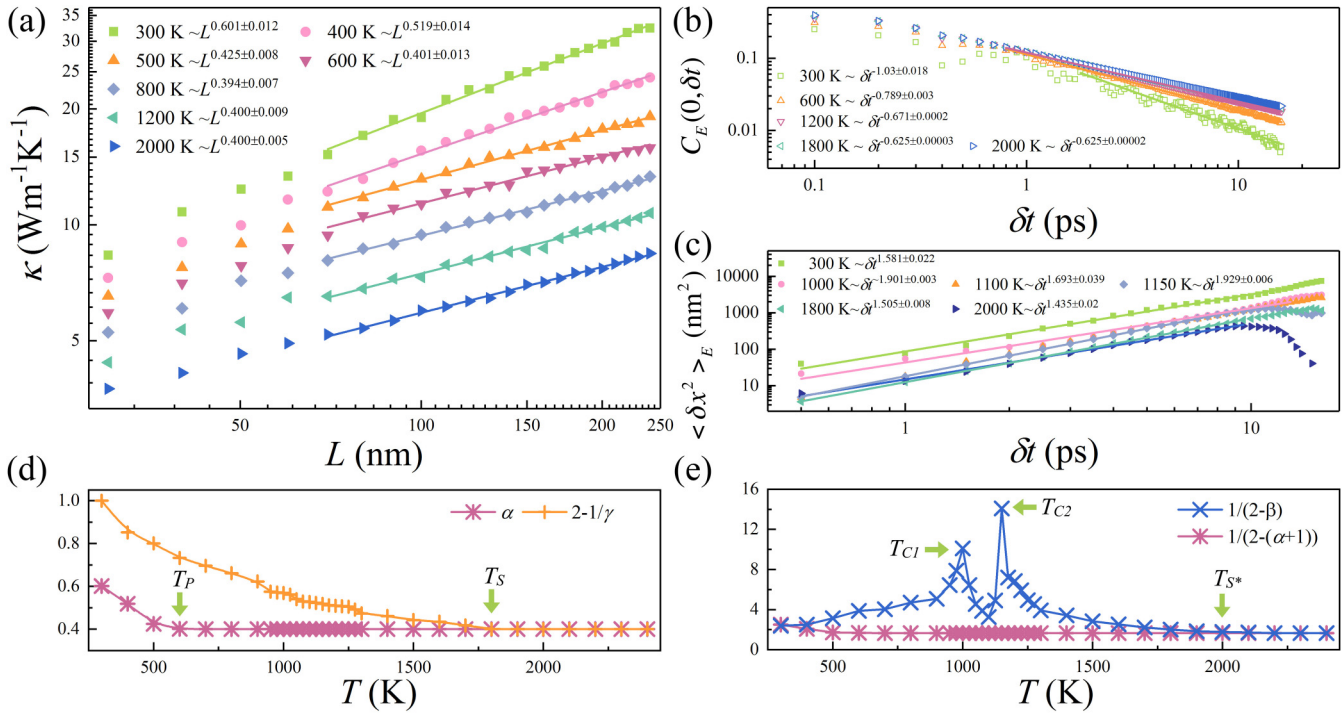


FIG. 5. (a–c) Thermal conductivity $\kappa$ diverges with length as $\sim L^{\alpha}$. Energy correlation peak $C_E(0, \delta t)$ decays with time as $\sim \delta t^{-\gamma}$. MSD of energy $\langle \delta x^2 \rangle_E$ increases with time as $\sim \delta t^{\beta}$. (d, e) Variations of $\alpha$, $\gamma$, and $\beta$ from 300 to 2400 K.

The considered length scale is far below the mean-free path of energy carriers where the quasi-one-dimensional $MoS_2$ is still within the ballistic-to-diffusive transition region of the energy carriers. It cannot answer whether thermal conduction is divergent or not in the infinite length scale. Similarly to carbon nanotubes [5], we conjecture that thermal conductivity of the quasi-one-dimensional $MoS_2$ might be convergent at a macroscopic length scale (e.g., in millimeter scale) since its out-of-plane motion would suppress the divergent nature of thermal conduction found in the strict one-dimensional system. Therefore a future study is thus heavily demanded to fully understand thermal conduction of $MoS_2$ in the macroscopic length scale.

## IV. CONCLUSION

In conclusion, we show a crossover of wave-packet dynamics and temperature-dependent anomalous energy transport, due to soliton excitations at high temperatures far below the melting point, in the quasi-one-dimensional $MoS_2$. The nonequilibrium wave-packet excitation and the equilibrium correlation of energy carriers are studied. The crossover process is characterized by an order parameter defined by the upper limit of energy transport speed and is related to a second-order phase transition. The crossover determines the variation of scaling exponents in the anomalous energy transport at a finite length scale within 2000 nm, which falls into the $\alpha = 2/5$ universality class and obeys the scaling relations $\alpha = 2 - 1/\gamma = \beta - 1$ in the soliton-dominated state. Our work sheds light on understanding the nonlinear dynamics and anomalous energy transport in low-dimensional crystalline solids.


## ACKNOWLEDGMENTS

This work was supported by the National Natural Science Foundation of China (#11405245) and the Natural Science Foundation of Shanghai (#14ZR1448100 and #19ZR1463200). The authors thank the Big Data Science Center of Shanghai Synchrotron Radiation Facility, the Shanghai Supercomputer Center of China, and the Supercomputing Center of the Chinese Academy of Sciences.


## APPENDIX

In this section, we shall demonstrate how to derive a KdV equation for a quasi-one dimensional $MoS_2$ system. As illustrated in Fig. 1(a), the schematic of the quasi-one-dimensional $MoS_2$ system is long the x axis. The continuum approximation method, usually applied in dealing with soliton solution in discrete lattices [26,27,42,43,46,66], is used by assuming small displacements from the equilibrium positions and a long wavelength limit.

First, The quasi-one-dimensional $MoS_2$ system is simplified as a one-dimensional chain with equal longitudinal atomic displacement in each periodic cell along the x axis. It means the empirical parameters are simplified to be identical between the periodic cells. The Hamiltonian of the one-dimensional chain has the form as [56–58],

$$H = \sum_i \frac{p_i^2}{2m_i} + \sum_{i\neq j, j>i} f_{ij}^C(r_{ij})[V^R(r_{ij}) - b_{ij}V^A(r_{ij})]$$
$$= \sum_i \frac{p_i^2}{2m_i} + \sum_{i\neq j, j>i} f_{ij}^C(r_{ij})\left[\left(1+\frac{Q}{r_{ij}}\right)Ae^{-\alpha r_{ij}} - b_{ij}Be^{-\beta r_{ij}}\right], \quad \text{(A1)}$$

where $p_i$ and $m_i$ denote the momentum and mass of $i$th atom, and $r_{ij}$ denotes the interatomic separation between $i$th and $j$th atom. Here, $Q$, $A$, $\alpha$, $B$, and $\beta$ are empirical pairwise parameters, which are simplified to be identical according to the average interactions between the periodic cells. Without this simplification, there would be three sets of empirical pairwise parameters for different covalent bonds (Mo-Mo, S-S and Mo-S). The cutoff function, $f_{ij}^C(r_{ij})$, is given by

$$f_{ij}^C(r_{ij}) = \begin{cases} 1, r_{ij} < R_{ij}^{\min} \\ \frac{1}{2}\left\{1 + \cos\left[\left(r_{ij} - R_{ij}^{\min}\right)\pi / \left(R_{ij}^{\max} - R_{ij}^{\min}\right)\right]\right\}, R_{ij}^{\min} < r_{ij} < R_{ij}^{\max} \\ 0, r_{ij} > R_{ij}^{\max}, \end{cases} \tag{A2}$$

where $R_{ij}^{\min}$ denotes a cutoff parameter. $V^R(r_{ij})$ and $V^A(r_{ij})$ are the pairwise repulsion and attraction, respectively. The bond order term, $b_{ij}$, describes the many-body interactions as $b_{ij} = [1 + \sum_{k\neq i,j} f_{ik}^C(r_{ik}) G[\cos(\theta_{ijk}) + P(N_i)]]^{\frac{1}{2}}$ according to a bond angle term $G$ and a coordinate term $P$. Here, $b_{ij}$ is also simplified as a constant parameter between the periodic cells in the atomic one-dimensional chain. The equation of motion for the $i$th atom is thus given,

$$\begin{aligned} \frac{\partial p_i}{\partial t} &= -\frac{\partial H}{\partial r_{ij}} \\ &= -\frac{\partial f_{ij}^C(r_{ij})}{\partial r_{ij}}\left[\left(1 + \frac{Q}{r_{ij}}\right)Ae^{-\alpha r_{ij}} - b_{ij}Be^{-\beta r_{ij}}\right] - f_{ij}^C(r_{ij}) \\ &\quad \times \left[-\frac{QA}{r_{ij}^2}e^{-\alpha r_{ij}} - \alpha A\left(1 + \frac{Q}{r_{ij}}\right)e^{-\alpha r_{ij}} + \beta b_{ij}Be^{-\beta r_{ij}}\right] \\ &= -\left(1 + \frac{Q}{r_{ij}}\right)Ae^{-\alpha r_{ij}}\frac{\partial f_{ij}^C(r_{ij})}{\partial r_{ij}} \\ &\quad + b_{ij}Be^{-\beta r_{ij}}\frac{\partial f_{ij}^C(r_{ij})}{\partial r_{ij}} + \frac{QA}{r_{ij}^2}e^{-\alpha r_{ij}}f_{ij}^C(r_{ij}) \\ &\quad + \alpha A\left(1 + \frac{Q}{r_{ij}}\right)e^{-\alpha r_{ij}}f_{ij}^C(r_{ij}) - \beta b_{ij}Be^{-\beta r_{ij}}f_{ij}^C(r_{ij}). \end{aligned} \tag{A3}$$

Hereafter, for simplicity, we set the atomic mass $m_i = 1$ and take spatial variables in units of the equilibrium bond length as 1, making them dimensionless. The right side of the equation of motions contains five parts and we shall expand them up to second-order of the interatomic displacement $r_{ij} - R_{ij}^{\min}$ to simplify this expression. First, the cutoff function and the interatomic separation are expanded as

$$f_{ij}^C(r_{ij}) = 1 - \frac{\pi^2}{4}\left(\frac{r_{ij} - R_{ij}^{\min}}{R_{ij}^{\max} - R_{ij}^{\min}}\right)^2 \tag{A4}$$

$$\begin{aligned} \frac{\partial f_{ij}^C(r_{ij})}{\partial r_{ij}} &= -\frac{\pi}{2\left(R_j^{\max} - R_{ij}^{\min}\right)} \\ &\quad \times \sin\left[\left(r_{ij} - R_{ij}^{\max}\right)\pi / \left(R_{ij}^{\max} - R_{ij}^{\min}\right)\right] \\ &= -\frac{\pi^2}{2\left(R_{ij}^{\max} - R_{ij}^{\min}\right)^2}\left(r_{ij} - R_{ij}^{\min}\right) \end{aligned} \tag{A5}$$

$$\begin{aligned} r_{ij}^a &= \left(R_{ij}^{\min} + r_{ij} - R_{ij}^{\min}\right)^a = \left(R_{ij}^{\min}\right)^a\left(1 + \frac{r_{ij} - R_{ij}^{\min}}{R_{ij}^{\min}}\right)^a \\ &= \left(R_{ij}^{\min}\right)^a\left[1 + a\frac{r_{ij} - R_{ij}^{\min}}{R_{ij}^{\min}} + \frac{a(a-1)}{2}\left(\frac{r_{ij} - R_{ij}^{\min}}{R_{ij}^{\min}}\right)^2\right], \\ a &= -1, -2. \end{aligned} \tag{A6}$$

where $a$ could be either $-1$ or $-2$. The two formulas are in the same form and thus we have simplified them into one formula as Eq. (A6).

Then we substitute the expressions (A4), (A5), and (A6) into the right side of the equation (A3) to get the expressions.

By doing so, we could get the first part in the right side of Eq. (A3) is obtained as

$$\begin{aligned} &-\frac{\partial f_{ij}^C(r_{ij})}{\partial r_{ij}}\left(1 + \frac{Q}{r_{ij}}\right)Ae^{-\alpha r_{ij}} \\ &= \frac{\pi^2 Ae^{-\alpha R_{ij}^{\min}}}{2\left(R_{ij}^{\max} - R_{ij}^{\min}\right)^2}\left(1 + \frac{Q}{R_{ij}^{\min}}\right)\left(r_{ij} - R_{ij}^{\min}\right) \\ &\quad - \frac{\pi^2 Ae^{-\alpha R_{ij}^{\min}}}{2\left(R_{ij}^{\max} - R_{ij}^{\min}\right)^2}\left[\alpha\left(1 + \frac{Q}{R_{ij}^{\min}}\right) + \frac{Q}{\left(R_{ij}^{\min}\right)^2}\right] \\ &\quad \times \left(r_{ij} - R_{ij}^{\min}\right)^2, \end{aligned} \tag{A7}$$

and the second part in the right side of Eq. (A3) is obtained as

$$\begin{aligned} -\frac{\partial f_{ij}^C(r_{ij})}{\partial r_{ij}}\left(-b_{ij}Be^{-\beta r_{ij}}\right) &= -\frac{\pi^2 b_{ij}Be^{-\beta R_{ij}^{\min}}}{2\left(R_{ij}^{\max} - R_{ij}^{\min}\right)^2}\left(r_{ij} - R_{ij}^{\min}\right) \\ &\quad + \frac{\pi^2 \beta b_{ij}Be^{-\beta R_{ij}^{\min}}}{2\left(R_{ij}^{\max} - R_{ij}^{\min}\right)^2}\left(r_{ij} - R_{ij}^{\min}\right)^2, \end{aligned} \tag{A8}$$

and the third part in the right side of Eq. (A3) is obtained as,

$$\begin{aligned} &-f_{ij}^C(r_{ij})\left(-\frac{QA}{r_{ij}^2}e^{-\alpha r_{ij}}\right) \\ &= -\frac{QAe^{-\alpha R_{ij}^{\min}}}{\left(R_{ij}^{\min}\right)^2}\left(\alpha + \frac{2}{R_{ij}^{\min}}\right)\left(r_{ij} - R_{ij}^{\min}\right) + \frac{QAe^{-\alpha R_{ij}^{\min}}}{\left(R_{ij}^{\min}\right)^2} \\ &\quad \times \left(-\frac{\pi^2}{4\left(R_{ij}^{\max} - R_{ij}^{\min}\right)^2} + \frac{3}{\left(R_{ij}^{\min}\right)^2} + \frac{2\alpha}{R_{ij}^{\min}} + \frac{\alpha^2}{2}\right) \\ &\quad \times \left(r_{ij} - R_{ij}^{\min}\right)^2 \end{aligned} \tag{A9}$$

and the fourth part in the right side of Eq. (A3) is obtained as

$$-f_{ij}^{C}(r_{ij})\left[-\alpha A\left(1+\frac{Q}{r_{ij}}\right)e^{-\alpha r_{ij}}\right]=-\alpha A e^{-\alpha R_{ij}^{\min}}\left[\frac{Q}{\left(R_{ij}^{\min}\right)^{2}}+\alpha\left(1+\frac{Q}{R_{ij}^{\min}}\right)\right]\left(r_{ij}-R_{ij}^{\min}\right)+\alpha A e^{-\alpha R_{ij}^{\min}}$$
$$\times\left[-\frac{\pi^{2}}{4\left(R_{ij}^{\max}-R_{ij}^{\min}\right)^{2}}\left(1+\frac{Q}{R_{ij}^{\min}}\right)+\frac{Q}{\left(R_{ij}^{\min}\right)^{3}}+\frac{\alpha^{2}}{2}\left(1+\frac{Q}{R_{ij}^{\min}}\right)+\frac{\alpha Q}{\left(R_{ij}^{\min}\right)^{2}}\right]\left(r_{ij}-R_{ij}^{\min}\right)^{2}, \tag{A10}$$

and the fifth part in the right side of Eq. (A3) is obtained as

$$-f_{ij}^{C}(r_{ij})(\beta b_{ij}Be^{-\beta r_{ij}})=\beta^{2}b_{ij}Be^{-\beta R_{ij}^{\min}}\left(r_{ij}-R_{ij}^{\min}\right)+\beta b_{ij}Be^{-\beta R_{ij}^{\min}}\left(\frac{\pi^{2}}{4\left(R_{ij}^{\max}-R_{ij}^{\min}\right)^{2}}-\frac{\beta^{2}}{2}\right)\left(r_{ij}-R_{ij}^{\min}\right)^{2}. \tag{A11}$$

Now we substitute the expression (A7)–(A11) into the right side of Eq. (A3) and omit the high-order terms to fully expand the equation of motions. It is derived an expression in the form of the first- and second-order terms of $r_{ij}-R_{ij}^{\min}$ as

$$\begin{aligned}\frac{\partial p_{i}}{\partial t}=&\frac{\pi^{2}Ae^{-\alpha R_{ij}^{\min}}}{2\left(R_{ij}^{\max}-R_{ij}^{\min}\right)^{2}}\left(1+\frac{Q}{R_{ij}^{\min}}\right)\left(r_{ij}-R_{ij}^{\min}\right)-\frac{\pi^{2}Ae^{-\alpha R_{ij}^{\min}}}{2\left(R_{ij}^{\max}-R_{ij}^{\min}\right)^{2}}\left[\alpha\left(1+\frac{Q}{R_{ij}^{\min}}\right)+\frac{Q}{\left(R_{ij}^{\min}\right)^{2}}\right]\left(r_{ij}-R_{ij}^{\min}\right)^{2}\\&-\frac{\pi^{2}b_{ij}Be^{-\beta R_{ij}^{\min}}}{2\left(R_{ij}^{\max}-R_{ij}^{\min}\right)^{2}}\left(r_{ij}-R_{ij}^{\min}\right)+\frac{\pi^{2}\beta b_{ij}Be^{-\beta R_{ij}^{\min}}}{2\left(R_{ij}^{\max}-R_{ij}^{\min}\right)^{2}}\left(r_{ij}-R_{ij}^{\min}\right)^{2}-\frac{QAe^{-\alpha R_{ij}^{\min}}}{\left(R_{ij}^{\min}\right)^{2}}\left(\alpha+\frac{2}{R_{ij}^{\min}}\right)\left(r_{ij}-R_{ij}^{\min}\right)+\frac{QAe^{-\alpha R_{ij}^{\min}}}{\left(R_{ij}^{\min}\right)^{2}}\\&\times\left(-\frac{\pi^{2}}{4\left(R_{ij}^{\max}-R_{ij}^{\min}\right)^{2}}+\frac{3}{\left(R_{ij}^{\min}\right)^{2}}+\frac{2\alpha}{R_{ij}^{\min}}+\frac{\alpha^{2}}{2}\right)\left(r_{ij}-R_{ij}^{\min}\right)^{2}-\alpha Ae^{-\alpha R_{ij}^{\min}}\left[\frac{Q}{\left(R_{ij}^{\min}\right)^{2}}+\alpha\left(1+\frac{Q}{R_{ij}^{\min}}\right)\right]\left(r_{ij}-R_{ij}^{\min}\right)\\&+\alpha Ae^{-\alpha R_{ij}^{\min}}\left[-\frac{\pi^{2}}{4\left(R_{ij}^{\max}-R_{ij}^{\min}\right)^{2}}\left(1+\frac{Q}{R_{ij}^{\min}}\right)+\frac{Q}{\left(R_{ij}^{\min}\right)^{3}}+\frac{\alpha^{2}}{2}\left(1+\frac{Q}{R_{ij}^{\min}}\right)+\frac{\alpha Q}{\left(R_{ij}^{\min}\right)^{2}}\right]\left(r_{ij}-R_{ij}^{\min}\right)^{2}\\&+\beta^{2}b_{ij}Be^{-\beta R_{ij}^{\min}}\left(r_{ij}-R_{ij}^{\min}\right)+\beta b_{ij}Be^{-\beta R_{ij}^{\min}}\left(\frac{\pi^{2}}{4\left(R_{ij}^{\max}-R_{ij}^{\min}\right)^{2}}-\frac{\beta^{2}}{2}\right)\left(r_{ij}-R_{ij}^{\min}\right)^{2}\\=&k_{1}\left(r_{ij}-R_{ij}^{\min}\right)+k_{2}\left(r_{ij}-R_{ij}^{\min}\right)^{2}.\end{aligned} \tag{A12}$$

The complete form of equation of motions is thus derived in the expressions of displacement variations. In order to simplify the complex form of equation of motions, here we define two constant parameters $k_1$ and $k_2$ in (A13) and (A14) to simplify,

$$\begin{aligned}k_{1}=&\frac{\pi^{2}Ae^{-\alpha R_{ij}^{\min}}}{2\left(R_{ij}^{\max}-R_{ij}^{\min}\right)^{2}}\left(1+\frac{Q}{R_{ij}^{\min}}\right)-\frac{\pi^{2}b_{ij}Be^{-\beta R_{ij}^{\min}}}{2\left(R_{ij}^{\max}-R_{ij}^{\min}\right)^{2}}-\frac{QAe^{-\alpha R_{ij}^{\min}}}{\left(R_{ij}^{\min}\right)^{2}}\left(\alpha+\frac{2}{R_{ij}^{\min}}\right)\\&-\alpha Ae^{-\alpha R_{ij}^{\min}}\left[\frac{Q}{\left(R_{ij}^{\min}\right)^{2}}+\alpha\left(1+\frac{Q}{R_{ij}^{\min}}\right)\right]+\beta^{2}b_{ij}Be^{-\beta R_{ij}^{\min}}\end{aligned} \tag{A13}$$

$$\begin{aligned}k_{2}=&-\frac{\pi^{2}Ae^{-\alpha R_{ij}^{\min}}}{2\left(R_{ij}^{\max}-R_{ij}^{\min}\right)^{2}}\left[\alpha\left(1+\frac{Q}{R_{ij}^{\min}}\right)+\frac{Q}{\left(R_{ij}^{\min}\right)^{2}}\right]+\frac{\pi^{2}\beta b_{ij}Be^{-\beta R_{ij}^{\min}}}{2\left(R_{ij}^{\max}-R_{ij}^{\min}\right)^{2}}\\&+\frac{QAe^{-\alpha R_{ij}^{\min}}}{\left(R_{ij}^{\min}\right)^{2}}\left(-\frac{\pi^{2}}{4\left(R_{ij}^{\max}-R_{ij}^{\min}\right)^{2}}+\frac{3}{\left(R_{ij}^{\min}\right)^{2}}+\frac{2\alpha}{R_{ij}^{\min}}+\frac{\alpha^{2}}{2}\right)\\&+\alpha Ae^{-\alpha R_{ij}^{\min}}\left[-\frac{\pi^{2}}{4\left(R_{ij}^{\max}-R_{ij}^{\min}\right)^{2}}\left(1+\frac{Q}{R_{ij}^{\min}}\right)+\frac{Q}{\left(R_{ij}^{\min}\right)^{3}}+\frac{\alpha^{2}}{2}\left(1+\frac{Q}{R_{ij}^{\min}}\right)+\frac{\alpha Q}{\left(R_{ij}^{\min}\right)^{2}}\right]\\&+\beta b_{ij}Be^{-\beta R_{ij}^{\min}}\left(\frac{\pi^{2}}{4\left(R_{ij}^{\max}-R_{ij}^{\min}\right)^{2}}-\frac{\beta^{2}}{2}\right).\end{aligned} \tag{A14}$$

Here, we only consider interactions between the nearest periodic cells as $j=i+1$ and $j=i-1$. The two terms of derivative of interactions, $r_{ij}-R_{ij}^{\min}$ and $(r_{ij}-R_{ij}^{\min})^2$, are expanded up to the fourth order of vibrational displacement

$r$ as,

$$r_{ii+1} - R_{ii+1}^{\min} = r + \frac{\partial r}{\partial x} + \frac{1}{2}\frac{\partial^2 r}{\partial x^2} + \frac{1}{6}\frac{\partial^3 r}{\partial x^3} + \frac{1}{24}\frac{\partial^4 r}{\partial x^4} \quad \text{(A15)}$$

$$r_{ii-1} - R_{ii-1}^{\min} = r - \frac{\partial r}{\partial x} + \frac{1}{2}\frac{\partial^2 r}{\partial x^2} - \frac{1}{6}\frac{\partial^3 r}{\partial x^3} + \frac{1}{24}\frac{\partial^4 r}{\partial x^4} \quad \text{(A16)}$$

$$\begin{aligned} r_{ij} - R_{ij}^{\min} &= \left(r_{ii+1} - R_{ii+1}^{\min}\right) - \left(r_{ii-1} - R_{ii-1}^{\min}\right) \\ &= \frac{2\partial r}{\partial x} + \frac{1}{3}\frac{\partial^3 r}{\partial x^3} \end{aligned} \quad \text{(A17)}$$

$$\left(r_{ij} - R_{ij}^{\min}\right)^2 = \left(r_{ii+1} - R_{ii+1}^{\min}\right)^2 - \left(r_{ii-1} - R_{ii-1}^{\min}\right)^2 = \frac{4r\partial r}{\partial x}. \quad \text{(A18)}$$

It is noted that $R_{ij}^{\min} = R_{ii+1}^{\min} = R_{ii-1}^{\min}$ is a constant and an opposite sign is added by calculating the derivative of interactions from the ($i$-1)th atom.

We substitute expressions (A15)–(A18) into the equation of motion (A12). It is derived as,

$$\frac{\partial p_i}{\partial t} = 2k_1\frac{\partial r}{\partial x} + 4k_2\frac{r\partial r}{\partial x} + \frac{1}{3}k_1\frac{\partial^3 r}{\partial x^3}. \quad \text{(A19)}$$

Now we introduce a small perturbation coefficient, $\varepsilon$, to describe the perturbation expansions as,

$$r = \varepsilon r_1 + \varepsilon^2 r_2 + \cdots, p_i = \varepsilon p_1 + \varepsilon^2 p_2 + \cdots. \quad \text{(A20)}$$

The space and time coordinates are transformed as

$$\varsigma = \varepsilon^{\frac{1}{2}}(x - v_0 t), \tau = \varepsilon^{\frac{3}{2}} t. \quad \text{(A21)}$$

Therefore, the laboratory derivatives of time and space are transformed as

$$\frac{\partial}{\partial t} = \frac{\partial}{\partial \varsigma}\frac{\partial \varsigma}{\partial t} + \frac{\partial}{\partial \tau}\frac{\partial \tau}{\partial t} = -v_0\varepsilon^{\frac{1}{2}}\frac{\partial}{\partial \varsigma} + \varepsilon^{\frac{3}{2}}\frac{\partial}{\partial \tau} \quad \text{(A22)}$$

$$\frac{\partial}{\partial x} = \frac{\partial}{\partial \varsigma}\frac{\partial \varsigma}{\partial x} = \varepsilon^{\frac{1}{2}}\frac{\partial}{\partial \varsigma}. \quad \text{(A23)}$$

Now we substitute expressions (A20)–(A23) into the equation of motions (A19). It is derived as

$$\begin{aligned} &\left(-v_0\varepsilon^{\frac{1}{2}}\frac{\partial}{\partial \varsigma} + \varepsilon^{\frac{3}{2}}\frac{\partial}{\partial \tau}\right)(\varepsilon p_1 + \varepsilon^2 p_2 + \cdots) \\ &= 2k_1\varepsilon^{\frac{1}{2}}\frac{\partial}{\partial \varsigma}(\varepsilon r_1 + \varepsilon^2 r_2 + \cdots) \\ &\quad + 4k_2(\varepsilon r_1 + \varepsilon^2 r_2 + \cdots)\varepsilon^{\frac{1}{2}}\frac{\partial}{\partial \varsigma}(\varepsilon r_1 + \varepsilon^2 r_2 + \cdots) \\ &\quad + \frac{1}{3}k_1\varepsilon^{\frac{3}{2}}\frac{\partial^3}{\partial \varsigma^3}(\varepsilon r_1 + \varepsilon^2 r_2 + \cdots). \end{aligned} \quad \text{(A24)}$$

Equating the terms of order $\varepsilon^{\frac{3}{2}}$ and $\varepsilon^{\frac{5}{2}}$, two equations are thus obtained,

$$-v_0\varepsilon^{\frac{3}{2}}\frac{\partial}{\partial \varsigma}p_1 = 2k_1\varepsilon^{\frac{3}{2}}\frac{\partial}{\partial \varsigma}r_1 \quad \text{(A25)}$$

$$\varepsilon^{\frac{5}{2}}\frac{\partial}{\partial \tau}p_1 = 4k_2\varepsilon^{\frac{5}{2}}r_1\frac{\partial}{\partial \varsigma}r_1 + \frac{k_1}{3}\varepsilon^{\frac{5}{2}}\frac{\partial^3}{\partial \varsigma^3}r_1. \quad \text{(A26)}$$

From Eq. (A25), a perturbation in the atomic chain is given as

$$\frac{\partial}{\partial \varsigma}(2k_1 r_1 + v_0 p_1) = 0, p_1 = -\frac{2k_2}{v_0}r_1. \quad \text{(A27)}$$

Next we substitute the solution (A27) into the equation (A26). It is derived as

$$\frac{\partial}{\partial \tau}\left(\frac{2k_1}{v_0}r_1\right) + 4k_2 r_1\frac{\partial r_1}{\partial \varsigma} + \frac{k_1}{3}\frac{\partial^3 r_1}{\partial \varsigma^3} = 0. \quad \text{(A28)}$$

We denote the derivation of $\dot{r}_1 = \frac{\partial r_1}{\partial \tau}$, $r_1^{\cdot} = \frac{\partial r_1}{\partial \varsigma}$ and $r_1^{\cdots} = \frac{\partial^3 r_1}{\partial \varsigma^3}$. The typical KdV equation is thus derived as

$$\dot{r}_1 + \frac{2v_0 k_2}{k_1}r_1 r_1^{\cdot} + \frac{v_0}{6}r_1^{\cdots} = 0. \quad \text{(A29)}$$

The one-soliton solution of the KdV equation (A27) is given as

$$r_1 = \frac{3v_s k_1}{4v_0 k_2}sech^2\sqrt{\frac{3v_s}{2v_0}}(\varsigma - v_s\tau), \quad \text{(A30)}$$

where $v_s$ is denoted as the soliton velocity. Hitherto the analytical feasibility of finding the soliton solutions in the quasi-one-dimensional $MoS_2$ is guaranteed.


[1] A. Dhar, Adv. Phys. **57**, 457 (2008).
[2] S. Lepri, R. Livi, and A. Politi, Phys. Rep. **377**, 1 (2003).
[3] R. Livi, J. Stat. Mech. (2020) 034001.
[4] Z. Zhang, Y. Ouyang, Y. Cheng, J. Chen, N. Li, and G. Zhang, Phys. Rep. **860**, 1 (2020).
[5] G. Barbalinardo, Z. Chen, H. Dong, Z. Fan, and D. Donadio, Phys. Rev. Lett. **127**, 025902 (2021).
[6] S. Lepri, Phys. Rev. E **58**, 7165 (1998).
[7] B. Li, H. Zhao, and B. Hu, Phys. Rev. Lett. **86**, 63 (2001).
[8] J.-S. Wang and B. Li, Phys. Rev. Lett. **92**, 074302 (2004).
[9] J.-S. Wang and B. Li, Phys. Rev. E **70**, 021204 (2004).
[10] A. V. Savin and Y. A. Kosevich, Phys. Rev. E **89**, 032102 (2014).
[11] S. Lepri, R. Livi, and A. Politi, Europhys. Lett. **43**, 271 (1998).
[12] L. Wang, Z. Wu, and L. Xu, Phys. Rev. E **91**, 062130 (2015).
[13] K. Aoki and D. Kusnezov, Phys. Rev. Lett. **86**, 4029 (2001).
[14] H. Zhao, Phys. Rev. Lett. **96**, 140602 (2006).
[15] O. Narayan and S. Ramaswamy, Phys. Rev. Lett. **89**, 200601 (2002).
[16] P. Grassberger, W. Nadler, and L. Yang, Phys. Rev. Lett. **89**, 180601 (2002).
[17] L. Delfini, S. Lepri, R. Livi, and A. Politi, Phys. Rev. E **73**, 060201(R) (2006).
[18] T. Mai, A. Dhar, and O. Narayan, Phys. Rev. Lett. **98**, 184301 (2007).
[19] H. van Beijeren, Phys. Rev. Lett. **108**, 180601 (2012).

[20] C. B. Mendl and H. Spohn, Phys. Rev. Lett. **111**, 230601 (2013).
[21] H. Spohn, J. Stat. Phys. **154**, 1191 (2014).
[22] S. Lepri, R. Livi, and A. Politi, Phys. Rev. Lett. **125**, 040604 (2020).
[23] S. Lepri, R. Livi, and A. Politi, Phys. Rev. Lett. **78**, 1896 (1997).
[24] G. Basile, C. Bernardin, and S. Olla, Phys. Rev. Lett. **96**, 204303 (2006).
[25] S. Tamaki, M. Sasada, and K. Saito, Phys. Rev. Lett. **119**, 110602 (2017).
[26] P. G. Drazin and R. S. Johnson, *Solitons: An Introduction*, 2nd ed. (Cambridge University Press, Cambridge, 1989).
[27] Y. S. Kivshar and B. A. Malomed, Rev. Mod. Phys. **61**, 763 (1989).
[28] D. W. Aossey, S. R. Skinner, J. L. Cooney, J. E. Williams, M. T. Gavin, D. R. Andersen, and K. E. Lonngren, Phys. Rev. A **45**, 2606 (1992).
[29] N. Theodorakopoulos and M. Peyrard, Phys. Rev. Lett. **83**, 2293 (1999).
[30] B. Hu, B. Li, and H. Zhao, Phys. Rev. E **61**, 3828 (2000).
[31] H. Zhao, Z. Wen, Y. Zhang, and D. Zheng, Phys. Rev. Lett. **94**, 025507 (2005).
[32] T. Jin, H. Zhao, and B. Hu, Phys. Rev. E **81**, 037601 (2010).
[33] R. K. Bullough and P. Caudrey, *Solitons*, Topics in Current Physics Vol. 17, 1st ed. (Springer-Verlag, Berlin Heidelberg, 1980).
[34] R. E. Peierls, *Quantum Theory of Solids* (Oxford University Press, London/New York, 2001).
[35] N. J. Zabusky and M. D. Kruskal, Phys. Rev. Lett. **15**, 240 (1965).
[36] N. Li, B. Li, and S. Flach, Phys. Rev. Lett. **105**, 054102 (2010).
[37] Y. Ming, L. Ye, H.-S. Chen, S.-F. Mao, H.-M. Li, and Z.-J. Ding, Phys. Rev. E **97**, 012221 (2018).
[38] Y. Ming, L. Ye, D.-B. Ling, H.-S. Chen, H.-M. Li, and Z.-J. Ding, Phys. Rev. E **98**, 032215 (2018).
[39] J. Wang and J. Chen, Phys. Rev. E **101**, 042207 (2020).
[40] N. Theodorakopoulos, Phys. Rev. Lett. **53**, 871 (1984).
[41] N. Theodorakopoulos and N. C. Bacalis, Phys. Rev. B **46**, 10706 (1992).
[42] S. Pnevmatikos, N. Flytzanis, and M. Remoissenet, Phys. Rev. B **33**, 2308 (1986).
[43] T. Y. Astakhova, O. D. Gurin, M. Menon, and G. A. Vinogradov, Phys. Rev. B **64**, 035418 (2001).
[44] C. W. Chang, D. Okawa, A. Majumdar, and A. Zettl, Science **314**, 1121 (2006).
[45] J. Chen, S. Chen, and Y. Gao, Phys. Rev. B **95**, 134301 (2017).
[46] T. Y. Astakhova, M. Menon, and G. A. Vinogradov, Phys. Rev. B **70**, 125409 (2004).
[47] K. F. Mak, C. Lee, J. Hone, J. Shan, and T. F. Heinz, Phys. Rev. Lett. **105**, 136805 (2010).
[48] Molybdenum Disulfide, PubChem. Retrieved August 31 (2018), https://pubchem.ncbi.nlm.nih.gov/compound/14823.
[49] P. Cipriani, S. Denisov, and A. Politi, Phys. Rev. Lett. **94**, 244301 (2005).
[50] L. Delfini, S. Denisov, S. Lepri, R. Livi, P. K. Mohanty, and A. Politi, Eur. Phys. J.: Spec. Top. **146**, 21 (2007).
[51] S. Liu, P. Hanggi, N. Li, J. Ren, and B. Li, Phys. Rev. Lett. **112**, 040601 (2014).
[52] A. Kundu and A. Dhar, Phys. Rev. E **94**, 062130 (2016).
[53] J. Wang, T.-X. Liu, X.-Z. Luo, X.-L. Xu, and N. Li, Phys. Rev. E **101**, 012126 (2020).
[54] V. Lee, C.-H. Wu, Z.-X. Lou, W.-L. Lee, and C.-W. Chang, Phys. Rev. Lett. **118**, 135901 (2017).
[55] R. Anufriev, S. Gluchko, S. Volz, and M. Nomura, ACS Nano **12**, 11928 (2018).
[56] T. Liang, S. R. Phillpot, and S. B. Sinnott, Phys. Rev. B **79**, 245110 (2009).
[57] T. Liang, S. R. Phillpot, and S. B. Sinnott, Phys. Rev. B **85**, 199903(E) (2012).
[58] K. Xu, A. J. Gabourie, A. Hashemi, Z. Fan, N. Wei, A. B. Farimani, H. P. Komsa, A. V. Krasheninnikov, E. Pop, and T. Ala-Nissila, Phys. Rev. B **99**, 054303 (2019).
[59] J. A. Stewart and D. E. Spearot, Modell. Simul. Mater. Sci. Eng. **21**, 045003 (2013).
[60] https://research.matse.psu.edu/sinnott/software.
[61] S. Chen, Y. Zhang, J. Wang, and H. Zhao, Phys. Rev. E **87**, 032153 (2013).
[62] F. Muller-Plathe, J. Chem. Phys. **106**, 6082 (1997).
[63] R. Holinski and J. Gansheimer, Wear **19**, 329 (1972).
[64] A. Kandemir, H. Yapicioglu, A. Kinaci, T. Cagın, and C. Sevik, Nanotechnology **27**, 055703 (2016).
[65] See Supplemental Material at http://link.aps.org/supplemental/10.1103/PhysRevB.104.224306 for PS1. Transverse Wave-packet Excitation; PS2. Longitudinal and Transverse Sound Speeds; PS3. Thermal Conductivity Calculations; PS4. Anomalous Energy Transport in the Zigzag $MoS_2$.
[66] M. Toda, Phys. Rep. **18**, 1 (1975).